Dynamically coupled plasmon-phonon modes in GaP: An indirect-gap polar semiconductor

Kunie Ishioka, Kristina Brixius, Ulrich Höfer, Avinash Rustagi, Evan M. Thatcher, Christopher J. Stanton, and Hrvoje Petek

Phys. Rev. B **92**, 205203 — Published 11 November 2015

DOI: 10.1103/PhysRevB.92.205203

Dynamically Coupled Plasmon-Phonon Modes in GaP; an Indirect-Gap, Polar Semiconductor

Kunie Ishioka*
Nano Characterization Unit, National Institute for Materials Science, Tsukuba, 305-0047 Japan

Kristina Brixius and Ulrich Höfer
Philipps-University, Material Sciences Center and Faculty of Physics, D-35032 Marburg, Germany

Avinash Rustagi, Evan M. Thatcher, and Christopher J. Stanton
Department of Physics, University of Florida, Gainesville, FL 32611 USA

Hrvoje Petek
Department of Physics and Astronomy and Pittsburgh Quantum Institute, University of Pittsburgh, Pittsburgh, PA 15260, USA
(Dated: October 14, 2015)

The ultrafast coupling dynamics of coherent optical phonons and the photoexcited electron-hole plasma in the indirect gap semiconductor GaP are investigated by experiment and theory. For below-gap excitation and probing by 800-nm light, only the bare longitudinal optical (LO) phonons are observed. For above-gap excitation with 400-nm light, the photoexcitation creates a high density, nonequilibrium $e-h$ plasma, which introduces an additional, faster decaying oscillation due to an LO phonon-plasmon coupled (LOPC) mode. The LOPC mode frequency exhibits very similar behavior for both n- and p-doped GaP, downshifting from the LO to the transverse optical (TO) phonon frequency limits with increasing photoexcited carrier density. We assign the LOPC mode to the LO phonons coupled with the photoexcited multi-component plasma. For the 400-nm excitation, the majority of the photoexcited electrons are scattered from Γ valley into the satellite X valley, while the light and spin-split holes are scattered into the heavy hole band, within 30 fs. The resulting mixed plasma is strongly damped, leading to the LOPC frequency appearing in the reststrahlen gap. Due to the large effective masses of the X electrons and heavy holes, the coupled mode appears most distinctly at carrier densities $\gtrsim 5 \times 10^{18}$ cm^{-3}. We perform theoretical calculations of the nuclear motions and the electronic polarizations following an excitation with an ultrashort optical pulse to obtain the transient reflectivity responses of the coupled modes. We find that, while the longitudinal diffusion of photoexcited carriers is insignificant, the lateral inhomogeneity of the photoexcited carriers due to the laser intensity profile should be taken into account to reproduce the major features of the observed coupled mode dynamics.

I. INTRODUCTION

Group III-V semiconductors have long been important materials with significant advantages over silicon in applications such as transistors[1], optical communications[2], solid state lighting[3], photocatalysis[4] and photovoltatics[5,6]. III-V semiconductors can have advantageous properties with respect to Si because of their direct band gaps, lower carrier masses, and shorter carrier lifetimes. In particular, the electron dynamics in III-V semiconductors are strongly affected by the interactions with the polar optical phonons, which contribute to ultrafast carrier momentum and energy scatterings[7–9].

In polar semiconductors like group III-V, Coulomb interaction between the collective oscillation of the electric charges (plasma) and the lattice polarization of the longitudinal optical (LO) phonons renormalizes their frequencies to give rise to LO phonon-plasmon coupled (LOPC) modes[10,11]. The LOPC modes have been studied by Raman scattering especially for GaAs[12–17]. Due to the band-dependent damping rates for electron and hole plasmas, the LOPC modes in n- and p-redtype semiconductors behave very differently. For n-type GaAs, for which the electron plasma damping is small compared with the LO phonon frequency ($\gamma_e \ll 2\pi\nu_{\rm LO}$), the LOPC mode appears as two branches above $\nu_{\rm LO}$ and below the transverse optical (TO) phonon frequency ($\nu_{\rm TO}$)[12]. Similar weakly damped LOPC modes have also been reported for other III-V semiconductors such as GaSb[18], InN[19], InP[20], InAs[21], and GaN[22]. For p-type GaAs, the LOPC mode appears within the reststrahlen gap between $\nu_{\rm LO}$ and $\nu_{\rm TO}$, because of the fast plasma damping ($\gamma_h > 2\pi\nu_{\rm LO}$) caused by the hole momentum scattering[14–17]. In other p-type III-V semiconductors[23–26], however, no such heavily damped LOPC modes have been reported.

GaP is another group III-V semiconductor with the same zinc-blende crystalline structure as GaAs. It is an indirect band-gap semiconductor with the fundamental gap at 2.26 eV, while its direct band gap at the Γ point is only slightly higher in energy (2.78 eV) [Fig. 1a]. This makes GaP an important material for light emitting diodes[30], photovoltatics[31] and water splitting photocatalysts[32] working in the visible range. Because GaP has a good epitaxial relationship with Si, it also provides an avenue for introducing optoelectronic functions into Si based devices, as well as for high-efficiency multi-junction solar cells[33–36]. The understanding of the carrier-lattice coupling under high density optical or electronic excitation is important for the function of the GaP devices. Nevertheless, the plasmon-phonon coupling of GaP is much less explored than GaAs. Previous Raman studies[37–40] reported that, as in GaAs, the LOPC frequency upshifted from $\nu_{\rm LO}$ upon n-type doping, though the lower branch was never observed. Upon p-type doping, the LOPC frequency of GaP upshifted slightly from $\nu_{\rm LO}$[39,40], contrary to the downshift that is established for p-type GaAs. It has remained uncertain, however, whether there is any fundamental difference in the LOPC mode behavior between GaP and GaAs. One may assume that there will be major differences in the plasmon-phonon couplings in these two systems, because the conduction band minimum is at the Γ point for GaAs and near the X points for GaP, with significantly different effective masses ($m_\Gamma = 0.063m_0$ for GaAs and $m_X = 0.30m_0$ for GaP, with m_0 being the free electron mass).

The LOPC modes in III-V semiconductors have also been observed as coherent oscillations in the time domain[41–46]. Being Raman-active, the coherent LO and LOPC modes can be excited with femtosecond optical pulses via the impulsive stimulated Raman scattering (ISRS) process[47,48]; this is the only generation mechanism for linear excitation below the band gap. In the case of above band-gap excitation, the coherent LO and LOPC modes can also be launched very efficiently via transient depletion field screening (TDFS)[41,49]. In this process, the photoexcited electrons and holes drift in the opposite direction and screen the surface built-in electric field instantaneously ($\ll$100 fs) [Fig. 2a,b]. This suddenly changes the equilibrium positions of the nuclei and excites the coherent LO phonons, which couple with plasma oscillations to form the coherent LOPC modes.

Pump-probe experiments have an advantage of being able to control the carrier density over a wide range without introducing lattice defects as one would do through impurity doping. By the choice of the pump-light wavelength and polarization, one can also selectively populate the satellite valleys in multi-valley semiconductors such as GaP and GaAs. In previous publications, we found that the plasmon-phonon coupling dynamics of n-type GaAs is drastically different between photoexcitations with 800-nm light[46] and with 400-nm light[50]; the LOPC mode appears at frequencies above $\nu_{\rm LO}$ and below $\nu_{\rm TO}$ for 800-nm excitation, but *between* $\nu_{\rm LO}$ and $\nu_{\rm TO}$ for 400-nm excitation. This is because the electrons are excited into different valleys, Γ with 800 nm and L with 400 nm, characterized by different effective masses and damping rates. The different excitation wavelengths also lead to different depth distributions of photoexcited carriers. The relatively short absorption length of the 400-nm light in GaAs promotes sub-picosecond diffusion of the photoexcited carriers away from the surface, causing the LOPC frequency to be time-dependent.

In the present study, we investigate the ultrafast dynamics of the coherent phonon-plasmon coupled mode in differently doped GaP samples for below and above band-gap excitation. For the below-gap excitation at 800 nm, only the bare LO phonon mode is observed regardless of the doping. When excited above the direct gap at 400 nm, by contrast, a distinct LOPC mode emerges as the pump density increases. The LOPC modes for the n- and p-type GaP exhibit similar behavior, with their frequencies shifting from $\nu_{\rm LO}$ to $\nu_{\rm TO}$ with increasing photoexcited carrier density. We attribute the LOPC modes of both the n- and p-type GaP to the LO phonon coupled with the photoexcited

multi-component plasma, consisting mainly of the X valley electrons and heavy holes. We calculate the transient reflectivity responses following excitation with an ultrashort optical pulse in the framework of the linear electro-optic effect. Unlike for GaAs, the carrier diffusion into the bulk is too slow to contribute to the carrier dynamics on the sub-picosecond time scale, but the time-dependent frequency is influenced by the laser beam profile, which determines the spatial distribution of photocarriers generated by the pump pulse, and how it is monitored by the probe pulse.

II. EXPERIMENTAL METHODS

The samples studied are (001)-oriented GaP wafers purchased from the MTI Corp. The doping with S and Zn impurities leads to n- and p-type conduction with $5\pm3\times10^{17}$ and 6.95×10^{17} cm^{-3} carrier densities, respectively. The undoped sample has n-type conduction with carrier concentration of $5\pm1\times10^{16}$ cm^{-3}. Hereafter we refer to the S-doped and Zn-doped samples as n- and p-doped.

Degenerate pump-probe reflectivity measurements are performed in ambient conditions with laser pulses of either 800- or 400-nm wavelength (1.55- or 3.1-eV photon energy) and 10 fs duration. Only the 400-nm photons can excite carriers across the direct band gap of GaP of 2.78 eV with a one-photon process, as shown in Fig. 1a. The electrons and holes photoexcited near the Γ point are scattered almost instantaneously ($\lesssim$30 fs) into the lower X (and to lesser extent, L) valleys[51,52] and into the heavy hole band. The optical penetration depth of the 400-nm light is given by α^{-1}=116 nm[53] with α the absorption coefficient, which is comparable with the thickness of the surface depletion layer of the n-doped sample, d=87 nm[54]. The probing depth of the 400-nm light is $(2\alpha)^{-1}$=58 nm, since the probe light passes the medium twice. In the case of 800-nm light, the probing depth is given by the reflection depth of a transparent medium $\lambda/2n\sim$126 nm, where λ is the optical wavelength and n is the index of refraction.

The pump-induced change in the anisotropic reflectivity ($\Delta R_{eo}=\Delta R_H-\Delta R_V$) is measured in the "electro-optic" (EO) configuration by detecting the difference between the vertically (V) and horizontally (H) polarized components of the reflected probe light using a balanced photodetector. The GaP crystals are oriented so that their [011] and [0$\overline{1}$1] axes are in the V and H directions. This detection scheme subtracts the largely isotropic non-oscillatory electronic response from the reflectivity signals and thereby allows us to detect the much smaller anisotropic oscillatory response with high sensitivity[46,55]. A spherical mirror brings the linearly polarized pump and probe beams to a common 23-μm diameter spot on the sample with angles of $<15^\circ$ and $<5^\circ$ from the surface normal. In this near back-reflection geometry from the (001) surface, the coherent TO phonon is neither excited nor detected according to the Raman selection rules[46]. The photoexcited carrier density is approximately given by $N=(1-R)F\alpha\lambda/hc$, where R is the reflectivity, $F=Q/(\pi d_b^2)$, the areal density of pump pulse energy, Q, the pump pulse energy, d_b, the laser spot radius, and hc/λ, the photon energy. The transient reflectivity signal is digitized and averaged with a 12-bit digital oscilloscope while time delay between pump and probe pulses is scanned repetitively at a 20 Hz rate.

III. EXPERIMENTAL RESULTS

A. Pump&probe with 800-nm light

We first examine the coherent response of GaP(001) when excited and probed nonresonantly with 800-nm light. The anisotropic reflectivity response of the n-doped GaP in Fig. 4 is modulated at the LO phonon frequency, which was previously reported in Raman and coherent phonon studies[38,45,56,57]. The amplitude $\Delta R_{\rm LO}$, the frequency $\nu_{\rm LO}$ and the dephasing rate $\Gamma_{\rm LO}$ of the coherent LO phonon are obtained by fitting the time domain data to a damped harmonic function:

$$\Delta R_{eo}(t)=\Delta R_{\rm LO}\exp(-\Gamma_{\rm LO}t)\sin(2\pi\nu_{\rm LO}t+\psi). \quad (1)$$

$\Delta R_{\rm LO}$ grows linearly with increasing pump density, whereas $\nu_{\rm LO}$=12.08 THz and $\Gamma_{\rm LO}$=0.08 ps^{-1} are independent of pump density, as expected for a non-resonant, one-photon process. The small dephasing rate is consistent with the previous reports[38,40,45]. When the pump polarization angle θ is rotated, the amplitude varies in proportion to $\cos 2\theta$, as shown in Fig. 3a. Because the ISRS force is expected to change directions with θ[46], we allow $\Delta R_{\rm LO}$ to be either positive or negative corresponding to the driving force direction, while keeping the initial phase ψ between 0 and π. The observed θ-dependence confirms the generation of coherent LO phonon to be via ISRS rather than TDFS, which is expected to be θ-independent.

The undoped and p-doped samples also show very similar reflectivity responses; no additional feature that could be attributed to the LOPC mode is observed. This is because the impurity-doped carrier density N in our samples

($N \lesssim 10^{17}$ cm^{-3}) is too low for effective coupling. The LOPC mode appears most appreciably when the plasma frequency:

$$\nu_p = \frac{\omega_p}{2\pi} = \frac{1}{2\pi}\sqrt{\frac{4\pi N e^2}{m^* \varepsilon_\infty}}, \tag{2}$$

shown inFig. 1b, is comparable with $\nu_{\rm LO}$. Here m^* is the carrier effective mass listed in Table I, and ε_∞=9.11 is the high frequency dielectric constant. For electrons in the conduction band minimum (X valley) and the holes in the valence band maximum (heavy holes), this would happen for electron and hole densities $N_e \sim 8 \times 10^{18}$ and $N_h \sim 1 \times 10^{19}$ cm^{-3}, respectively.

B. Pump&probe with 400-nm light

Next we examine the coherent response under resonant photoexcitation and probing with 400-nm light. For n- and p-doped GaP, a new fast decaying oscillation component grows with increasing pump density, while the long-lived LO phonon appears unchanged, as shown in Fig. 4. The fast decaying oscillation appears also for undoped GaP, though only at the highest pump densities examined and with small amplitude. We fit the oscillatory part of the reflectivity with the linear combination of two damped harmonic functions:

$$\begin{aligned}\Delta R_{eo}(t) =& \Delta R_{\rm LOPC} \exp(-\gamma_{\rm LOPC} t) \sin[(2\pi\nu_{\rm LOPC} + \beta t)t + \varphi] \\ &+ \quad \Delta R_{\rm LO} \exp(-\Gamma_{\rm LO} t) \sin(2\pi\nu_{\rm LO} t + \psi).\end{aligned} \tag{3}$$

Here we approximate the time-dependent frequency with a linear chirp β, though its actual time-evolution is more complicated, as we will show later in this section. The fast decaying oscillations of differently doped GaP samples behave very similarly with increasing carrier density, as plotted in Fig. 5; $\nu_{\rm LOPC}$ downshifts from the $\nu_{\rm LO}$ toward the $\nu_{\rm TO}$ limits, whereas $\gamma_{\rm LOPC}$ becomes maximum at $N \sim 1 \times 10^{19}$ cm^{-3}. The carrier density-dependent frequency confirms that the fast decaying oscillation is an LOPC mode of the photoexcited plasma; the similarity among differently doped GaP suggests that the same photoexcited plasma is responsible.

The LOPC amplitude $\Delta R_{\rm LOPC}$ increases with increasing carrier density N, until it reaches a saturation at $N \sim 1 \times 10^{19}$ cm^{-3}, as shown in Fig. 6a. The saturation is attributed to the complete screening of the built-in electric field by the ultrafast drift of photoexcited carriers in the TDFS mechanism [Fig. 2b]. The dominance of the TDFS in the LOPC generation is evidenced by the pump polarization-dependence of $\Delta R_{\rm LOPC}$ [Fig. 3b]. $\Delta R_{\rm LOPC}$ can be fitted to $A + B\cos 2\theta$ with $A \sim 10B$, indicating that the contribution of the TDFS generation is 10 times larger than that of the ISRS. The LO amplitude $\Delta R_{\rm LO}$, by contrast, hardly grows with carrier density [Fig. 6b]. We consider that the bare LO phonons arise mainly from the low-density rim of the inhomogeneous laser spot, as we will discuss in Sect. IV D.

To examine the dynamical aspects of plasma-phonon coupling through the time-dependent LOPC frequency, we perform time-windowed FT analysis of the coherent oscillation signals. Figure 7 plots the FT amplitude as a function of the position of the time window and frequency. We see that the peak frequency, which includes both LO and LOPC contributions, shows a more complicated time-dependence than a linear function. For the n- and p-doped GaP, the peak frequency stays at a constant value between $\nu_{\rm TO}$ and $\nu_{\rm LO}$ for ∼0.3 ps, and then approaches $\nu_{\rm LO}$ as the LOPC amplitude decays; after that the signal consists of only the bare LO phonon mode. In the case of the undoped GaP, the frequency exhibits even more complicated time-evolution. Though it starts from the similar frequency as that of the n-doped GaP, it upshifts quickly *above* $\nu_{\rm LO}$ before finally converging to $\nu_{\rm LO}$. In fact, the frequency overshoot above $\nu_{\rm LO}$ occurs also for p-doped GaP, though less prominently. If we examine the chronograms in Fig. 7 closely, we notice that the frequency overshoots are accompanied by the anti-resonance (dip) at $\sim \nu_{\rm TO}$. Such dips can be manifestations of the destructive interferences between oscillations with slightly different frequencies and phases[58]. We therefore consider that the frequency overshoots are the consequence of the destructive interference pushing the amplitude maxima above $\nu_{\rm LO}$, rather than the LOPC mode shooting above $\nu_{\rm LO}$. We will discuss the possible origins of this complex behavior in the following section.

IV. THEORY AND MODELING

A. Coupled plasmon-phonon eigenmodes

We model the temporal and spatial behavior of LOPC mode of GaP taking into account electrons and holes excited in multiple conduction and valence bands. The excitation of GaP with 400-nm light involves transitions from the

heavy, light and split-off hole valence bands into the Γ valley of the conduction band, as shown in Fig. 1a. However, the electrons are scattered from the Γ valley primarily into the X valley and, to the lesser extent, into the L valleys[51,52], whereas the holes are scattered into the heavy hole band, before they form the plasmon-phonon coupled mode ($\lesssim$ 100 fs). This makes the situation similar to GaAs photoexcited with 400-nm light, where the mixed plasma of the L electrons and the heavy holes dominate the plasmon-phonon coupling. We therefore approximately describe the multi-component plasma of GaP by a single component with an effective mass and damping rate, as we did in the case of GaAs[50]. We use $m_{\rm eh}^{-1} = m_{\rm X}^{-1} + m_{HH}^{-1}$ as the effective mass of the mixed plasma, with m_X and m_{HH} being the effective masses of the X electrons and heavy holes listed in Table I.

The transient response of the LOPC mode is obtained by solving the equations for coupled plasmon-phonon modes:

$$\begin{aligned}\frac{\partial^2 \mathbf{P}}{\partial t^2} + \gamma_p \frac{\partial \mathbf{P}}{\partial t} + \omega_p^2 \mathbf{P} &= \frac{e^2 N(t)}{\varepsilon_\infty m_p}(\mathbf{E}^{\rm ext} - 4\pi\gamma_{12}\mathbf{W}) \\ \frac{\partial^2 \mathbf{W}}{\partial t^2} + \Gamma \frac{\partial \mathbf{W}}{\partial t} + \Omega_{\rm LO}^2 \mathbf{W} &= \frac{\gamma_{12}}{\varepsilon_\infty}(\mathbf{E}^{\rm ext} - 4\pi\mathbf{P}).\end{aligned} \tag{4}$$

Here $\mathbf{P}$ is the electronic polarization, $\mathbf{W} = (\sqrt{\rho})\mathbf{u}$ is the normalized lattice displacement with $\mathbf{u}$ and ρ being the optical phonon mode displacement and density, $\mathbf{E}^{\rm ext}$ is a statically applied electric field or the surface depletion field. $\Gamma = 2\Gamma_{\rm LO}$ is the phonon population decay rate, γ_p and m_p are the plasmon damping rate and effective mass, $\Omega_{\rm LO} = 2\pi\nu_{\rm LO}$ and $\Omega_{\rm TO} = 2\pi\nu_{\rm TO}$. The coupling constant between the plasmons and the phonons is given by $\gamma_{12} = \Omega_{\rm TO}\sqrt{(\varepsilon_0 - \varepsilon_\infty)/4\pi}$ with ε_0=11.1 being the static dielectric constant. The coupling for GaP, $\gamma_{12}/2\pi$=4.36 THz, is slightly larger than that for GaAs, 3.22 THz[53].

We first consider static situations by neglecting the external field and writing $\mathbf{P}$=$\mathbf{P}_0 e^{-i\omega t}$ and $\mathbf{W}$=$\mathbf{W}_0 e^{-i\omega t}$ with complex ω. We find a fourth-order equation for the eigenmodes of eq. (4)[50], which is formally equivalent to solving for the zeros of the dielectric function[16,17,38]:

$$\varepsilon(\omega) = \varepsilon_\infty \Big[1 + \frac{\Omega_{\rm LO}^2 - \Omega_{\rm TO}^2}{\Omega_{\rm TO}^2 - i\Gamma\omega - \omega^2} - \frac{\omega_p^2}{\omega^2 + i\gamma_p\omega}\Big]. \tag{5}$$

This leads to the LOPC frequency appearing above the LO and below the TO frequencies for nearly undamped ($\gamma_p \ll \Omega_{\rm TO}$) plasma, and between LO and TO frequencies for heavily damped ($\gamma_p > \Omega_{\rm TO}$) plasma, as summarized in Fig. 8a.

Though eq. (5) cannot treat transient responses to the photoexcitation, it can give us some insight into the coupled-mode dynamics. On one hand, the real part of the solution, Re(ω), reproduces the experimentally observed $\nu_{\rm LOPC}$ excellently, as shown with the solid curve in Fig. 5a, in the case of the plasma damping of $\gamma_p/2\pi$=25 THz. This damping rate suggests that the the equilibration between the Γ, L and X valleys is achieved as fast as 50 fs due to a large density of states contributing to the momentum scattering. On the other hand, the imaginary part Im(ω) reproduces the experimental $\gamma_{\rm LOPC}$ only roughly. The quantitative discrepancy between experimental and theoretical damping rates is attributed to the time-dependence and the spatial inhomogeneity of the carrier density, which we have so far neglected but will consider in the following subsections.

B. Transient reflectivity signals

We now calculate the differential reflectivity signal arising from the excitation of the coupled mode including the effects of the initial transients. The coupled plasmon-phonon mode equations [eq. (4)] are numerically solved with the following initial conditions. In the absence of photoexcited carriers (for $t < 0$), the electronic polarization $\mathbf{P}$ is zero, whereas the normalized lattice displacement $\mathbf{W}$ has a finite value caused by the electric field:

$$\begin{aligned}\mathbf{P} &= 0, \\ \mathbf{W} &= \frac{\gamma_{12}\mathbf{E}^{ext}}{\varepsilon_\infty \Omega_{\rm LO}^2}.\end{aligned} \tag{6}$$

At t=0, an ultrashort pump pulse creates photoexcited carriers, which screen the surface field $\mathbf{E}_{ext}$ either partially or completely, depending on the carrier density N. In the case of complete screening, the system will evolve over time to a new steady state given by:

$$\begin{aligned}\mathbf{P} &= \frac{\mathbf{E}^{ext}}{4\pi}, \\ \mathbf{W} &= 0.\end{aligned} \tag{7}$$

In the case of imcomplete screening, **P** and **W** take intermediate values between eqs. (6) and (7) in proportion to N. This sudden change in the polarization and equilibrium position launches coherent oscillations in both polarization and lattice displacement.

The transient reflectivity signal for $t > 0$ consists of the contributions from the electric field and the nuclear displacement[49]:

$$\frac{\Delta R(t)}{R} \propto r^e E(t) + r^w \Big[W(t) \frac{\Omega_{\rm LO}^2 \varepsilon_\infty}{\gamma_{12}} \Big]; \\ E(t) = E^{ext} - 4\pi P(t) - 4\pi\gamma_{12} W(t). \tag{8}$$

Here r^e and r^w represent the weights of the electronic and nuclear contributions, with the theoretically calculated ratio of $r^e/r^w = -2.1$ for GaP[59].

C. Carrier Diffusion

The theoretical modeling presented so far has neglected the time evolution of the carrier density after photoexcitation. In the case of GaAs excited with 400-nm light[50], we found the coupled mode frequency to depend on time on sub-picosecond scale because of the decay in the carrier density at the surface through ambipolar diffusion. Here we examine the effect of the ambipolar diffusion for GaP by calculating the coupled mode frequency at the surface as a function of time.

The photoexcited carriers initially have a density distribution expressed by $N(z, t = 0) = N_0 e^{-\alpha z}$ with respect to the distance z from the surface. After the ultrafast but incomplete charge separation illustrated in Fig. 2b, both electrons and holes diffuse away from the surface (ambipolar diffusion), as schematically shown in Fig. 2c, since both carriers have still considerable density gradients with respect to z. The ambipolar diffusion coefficient is given by $D_{\rm am} = (\mu_h D_e + \mu_e D_h)/(\mu_e + \mu_h)$, where D_e and D_h are the electron and hole diffusion constants, and μ_e and μ_h are the corresponding carrier mobilities. We estimate the ambipolar diffusion coefficient to be $5 - 10$ cm^{2}s^{-1} using $D_e < 6.5$ cm^2 s^{-1}, $D_h < 4$ cm^2 s^{-1} and assuming the electron mobility is of the same order of magnitude as the hole mobility. The obtained diffusion coefficient is smaller than what we estimated for GaAs, $15 - 30$ cm^2 s^{-1}[50].

The carrier density at the surface $N(z = 0, t)$ and the corresponding coupled mode frequency are calculated as a function of time t using the same formulae as in our previous study for GaAs[50]. We find that the carrier density decays on several ps time scale, and consequently the coupled mode frequency hardly varies within 1 ps, as shown in Fig. 9. This is in contrast with our experimental observation, in which the LOPC frequency upshifts toward $\nu_{\rm LO}$ in *sub*-ps time scale [Fig. 7]. We therefore conclude that the ambipolar diffusion plays no important role in the time evolution of the LOPC frequency of GaP. Because the frequency upshifts as the LOPC amplitude decreases, we attribute the upshift mainly to the dephasing (disappearance) of the LOPC mode, after which we see only the bare LO phonon.

D. Lateral Inhomogeneity

Besides the carrier density distribution in the depth direction, there is also inhomogeneity in the lateral direction due to the Gaussian intensity profiles of the laser. Since the frequency and dephasing rate of the coupled mode strongly depend on the carrier density, as shown in Fig. 8, the inhomogeneity would lead to the coherent superposition of reflectivity signals with a laterally varying frequency and dephasing rate. This would imply the signal from the high-density center of the laser spot to have a frequency $\sim \nu_{\rm TO}$ and fast dephasing rate, and that from the low-density rim to have frequency $\sim \nu_{\rm LO}$ and live longer, in the case of relatively intense excitation.

We calculate the reflectivity transients including the effect of lateral inhomogeneity both in the pump and probe laser spots. The reflectivity transient $\Delta R(t)$ for a single carrier density N is given by eq. (8). Here we consider position-dependent transients $\Delta R[t, N(r)]$, with r being the distance from the center of the laser spot and $N(r) = N(r, t = 0) = N_{max} \exp(-r^2/d_b^2)$ proportional to the intensity profile of the laser spot $G(r) = G_{max} \exp(-r^2/d_b^2)$. To obtain the total reflectivity transients $\Delta R^{tot}(t)$ we need to average $\Delta R[t, N(r)]$ with weight of probe light field[60]. This yields :

$$\Delta R^{tot}(t) \propto \int_0^\infty 2\pi r dr \Delta R[t, N(r)] \sqrt{N(r)}, \tag{9}$$

since the field is proportional to the square root of the intensity, $\sqrt{G(r)}$, and therefore to that of the carrier density,

$\sqrt{N(r)}$. The spatial integral can be translated to an integral over the number density using the relation $dN \propto N(r)rdr$:

$$\Delta R^{tot}(t) \propto \int_0^{N_{max}} dN \frac{\Delta R(t,N)}{\sqrt{N}}, \tag{10}$$

where $N_{max} = N(r = 0, t = 0)$. The calculated transient reflectivity traces, shown in Fig. 10 together with their FT spectra, reproduce the overall features of the experimentally observed responses in Fig. 4.

Figure 11 compares the time-windowed FT spectrum of the transient reflectivity calculated with and without the effect of the lateral inhomogeneity. The calculation including the inhomogeneity reproduces the experimental observation in Fig. 7 well, with the peak frequency first staying at a nearly constant value near $\nu_{\rm TO}$ and then jumping up to $\nu_{\rm LO}$ at around 0.5 ps with a clear overshoot. In Figs. 11b as well as 7b,c we see that a dip in the amplitude causes the frequency overshoot above $\nu_{\rm LO}$. This dip is a consequence of the superpositions among the LOPC modes with different frequencies, damping rates and phases, which are integrated over the laser spot profile.

V. DISCUSSION

Photo-doping of carriers into semiconductors can induce effects similar to impurity doping, except that it always creates a multi-component plasma, *i.e.*, both electrons *and* holes in different conduction and valence bands, instead of one. In the case of n-doped GaAs photoexcited with 800-nm light, electron-hole pairs are created across the fundamental gap at the Γ point. Because of the vastly different damping rates of the two types of carriers (γ_h=25 THz and γ_e=0.1 THz[44]), two distinct coupled modes, one coupled with the Γ valley electrons and another coupled with the holes, are observed at separate frequencies[44,46]. The situation is different for GaAs excited with 400-nm light[50]. In this case, electron-hole pairs are initially created in the L valley and with large excess energy in the Γ valley, followed by intra- and intervalley scatterings that relocate electrons and holes predominantly into the L valley and the heavy hole band. Because the damping of the L electrons is nearly as fast as that of the heavy holes, the multi-component plasma coupled with the LO phonons is observed as an effectively single-component, heavily damped plasma. Moreover, strong absorption of the excitation light leads to a steep depth distribution of photoexcited carriers, which, together with a relatively large diffusion coefficient, causes the ambipolar diffusion to play a major role in the coupled mode dynamics on the sub-picosecond time scale.

In the case of GaP excited with 400-nm light, we also observe only one LOPC mode. The 400-nm light initially creates electron-hole pairs in the Γ valley, as shown in Fig. 1a. Previous studies[51,52] suggest, however, that the photoexcited electrons are scattered from the Γ into the lower-lying X (and L) valleys, whereas the light holes are scattered into the heavy hole band, within 30 fs. The X electrons and heavy holes are therefore expected to dominate the coupled mode dynamics of GaP, like the L electrons and heavy holes for GaAs. A major difference between GaP and GaAs lies, however, in the penetration depths (α^{-1}) of the 400-nm light, which is eight times larger in GaP than in GaAs. This makes the initial depth distribution of photoexcited carriers less steep for GaP than GaAs, and, together with a relatively small diffusion coefficient, makes the effect of the ambipolar diffusion less prominent in the case of GaP.

Our observation of the LOPC mode for n- and p-doped GaP, both appearing with similar dephasing rates and frequencies [Fig. 5], confirms that the same photoexcited multi-component plasma is responsible for the coupled mode. Time evolution of the coupled mode frequency [Fig. 7] exhibits clear doping dependence, however; the transient frequency shift above $\Omega_{\rm LO}$ is distinct for undoped GaP, less so for p-doped GaP, and not observed for n-doped GaP. This appears puzzling at first glance, since the reflectivity responses calculated by eq. (6-8) are symmetric about $\mathbf{E}^{ext}$ and reversing the sign of the surface field should not affect the transient reflectivity response. Varying the doping type also modifies the *magnitude and depth* of the surface field, however. Though we have considered only the carrier density at the surface ($z = 0$) in Fig. 9, the actual reflectivity signals have contributions also from inhomogeneity in the depth direction, since the absorption depth (α^{-1}) of 400-nm light is comparable with the surface depletion width (d). Differences in the surface field could therefore lead to the difference in the plasma dynamics, and thereby in time-evolution of the LOPC frequency, between the n- and p-doped samples. Inclusion of the effect of the longitudinal inhomogeneity on the reflectivity signals is beyond the scope of this paper.

VI. CONCLUSION

We have observed coherent LO phonons of GaP for below-gap photoexcitation at 800 nm, and both the LO and LOPC modes for above-gap excitation at 400 nm. The LOPC mode are assigned as the LO phonon coupled with photoexcited multi-component plasma consisting mainly of the electrons in the X valleys and heavy holes. The overall

behavior of the LOPC mode is similar to that observed for GaAs photoexcited at 400 nm, whose carrier dynamics are dominated by the L electrons and heavy holes. For GaP, however, the effect of the ambipolar diffusion is less significant than for GaAs because of the larger penetration depth and smaller diffusion coefficient. This allows us to observe the effect of the lateral inhomogeneity within the laser spots, which could not be separated from the effect of carrier diffusion for GaAs, distinctly for GaP. The obtained insight will contribute to understanding the carrier-phonon interaction of group III-V semiconductors at extremely high doping densities under non-equilibrium conditions.

ACKNOWLEDGMENTS

This work is partly supported by the Deutsche Forschungsgemeinschaft through SFB 1083 and HO2295/8 and by NSF grant DMR-1311845 (Petek) and DMR-1311849 (Stanton). HP thanks support from the Alexander von Humboldt Foundation and the Chinese Academy of Sciences President's International Fellowship Initiative.

* ishioka.kunie@nims.go.jp

[1] J. del Alamo, Nature **479**, 317 (2011).
[2] T. Ibrahim, W. Cao, Y. Kim, J. Li, J. Goldhar, P. Ho, and C. Lee, Photon. Tech. Lett., IEEE **15**, 36 (2003).
[3] M. Kneissl, T. Kolbe, C. Chua, V. Kueller, N. Lobo, J. Stellmach, A. Knauer, H. Rodriguez, S. Einfeldt, Z. Yang, N. Johnson, and M. Weyers, Semicond. Sci. Tech. **26**, 014036 (2011).
[4] J. Li and N. Wu, Catalysis Sci. Tech. **5**, 1360 (2015).
[5] S. Philipps, F. Dimroth, and A. Bett, in *Practical Handbook of Photovoltaics* (Elsevier, 2012) pp. 417–446.
[6] R. LaPierre, A. Chia, S. Gibson, C. Haapamaki, J. Boulanger, R. Yee, P. Kuyanov, J. Zhang, N. Tajik, N. Jewell, and K. Rahman, phys. stat. sol. RRL **7**, 815 (2013).
[7] A. Othonos, J. Appl. Phys. **83**, 1789 (1998).
[8] V. Axt and T. Kuhn, Rep. Prog. Phys. **67**, 433 (2004).
[9] R. Ulbricht, E. Hendry, J. Shan, T. Heinz, and M. Bonn, Rev. Mod. Phys. **83**, 543 (2011).
[10] I. Yokota, J. Phys. Soc. Jpn. **16**, 2075 (1961).
[11] B. B. Varga, Phys. Rev. **137**, A1896 (1965).
[12] A. Mooradian and A. L. McWhorter, Phys. Rev. Lett. **19**, 849 (1967).
[13] V. Vorlicek, I. Gregora, W. Kauschke, J. Menendez, and M. Cardona, Phys. Rev. B **42**, 5802 (1990).
[14] K. Wan and J. Young, Phys. Rev. B **41**, 10772 (1990).
[15] A. Mlayah, R. Carles, G. Landa, E. Bedel, and A. Munoz-Yague, J. Appl. Phys. **69**, 4064 (1991).
[16] R. Fukasawa and S. Perkowitz, Phys. Rev. B **50**, 14119 (1994); Jpn. J. Appl. Phys. **35**, 132 (1996).
[17] G. Irmer, M. Wenzel, and J. Monecke, Phys. Rev. B **56**, 9524 (1997).
[18] W. Kauschke, N. Mestres, and M. Cardona, Phys. Rev. B **36**, 7469 (1987).
[19] R. Cusco, J. Ibanez, E. Alarcon-Llado, L. Artus, T. Yamaguchi, and Y. Nanishi, Phys. Rev. B **79**, 155210 (2009).
[20] W. Kauschke and M. Cardona, Phys. Rev. B **33**, 5473 (1986).
[21] S. Buchner and E. Burstein, Phys. Rev. Lett. **33**, 908 (1974).
[22] P. Perlin, J. Camassel, W. Knap, T. Taliercio, J. Chervin, T. Suski, I. Grzegory, and S. Porowski, Appl. Phys. Lett. **67**, 2524 (1995).
[23] M. Qi, M. Konagai, and K. Takahashi, J. Appl. Phys. **78**, 7265 (1995).
[24] A. Mintairov and H. Temkin, Phys. Rev. B **55**, 5117 (1997).
[25] H. Harima, T. Inoue, S. Nakashima, K. Furukawa, and M. Taneya, Appl. Phys. Lett. **73**, 2000 (1998).
[26] F. Demangeot, J. Frandon, M. Renucci, N. Grandjean, B. Beaumont, J. Massies, and P. Gibart, Solid State Commun. **106**, 491 (1998).
[27] D. W. Bailey, C. J. Stanton, and K. Hess, Phys. Rev. B **42**, 3423 (1990).
[28] M. Cardona and F. H. Pollak, Phys. Rev. **142**, 530 (1966).
[29] J. R. Chelikowsky and M. L. Cohen, Phys. Rev. B **14**, 556 (1976).
[30] A. Bergh and P. Dean, Proceedings of the IEEE **60**, 156 (1972).
[31] X. Lu, S. Huang, M. Diaz, N. Kotulak, H. Ruiying, R. Opila, and A. Barnett, IEEE J. Photovoltaics **2**, 214 (2012).
[32] J. Sun, C. Liu, and P. Yang, J. Am. Chem. Soc. **133**, 19306 (2011).
[33] K. Volz, A. Beyer, W. Witte, J. Ohlmann, I. Nemeth, B. Kunert, and W. Stolz, J. Crystal Growth **315**, 37 (2011).
[34] T. Thanh, C. Robert, W. Guo, A. Letoublon, C. Cornet, G. Elias, A. Ponchet, T. Rohel, N. Bertru, A. Balocchi, O. Durand, J. Micha, M. Perrin, S. Loualiche, X. Marie, and A. Corre, J. Appl. Phys. **112**, 053521 (2012).
[35] A. Lin, M. Fejer, and J. Harris, J. Crystal Growth **363**, 258 (2013).
[36] O. Supplie, M. May, G. Steinbach, O. Romanyuk, F. Grosse, A. Nägelein, P. Kleinschmidt, S. Brückner, and T. Hannappel, J. Phys. Chem. Lett. **6**, 464 (2015).
[37] D. Hon and W. Faust, Appl. Phys. **1**, 241 (1973).
[38] G. Irmer, V. Toporov, B. Bairamov, and J. Monecke, phys. stat. sol. b , 595 (1983).

[39] M. Giehler and E. Jahne, phys. stat. sol. b **73**, 503 (1976).
[40] S. Nakashima, H. Yugami, A. Fujii, M. Hangyo, and H. Yamanaka, J. Appl. Phys. **64**, 3067 (1988).
[41] M. Först and T. Dekorsy, in *Coherent Vibrational Dynamics*, Practical Spectroscopy, edited by S. D. Silvestri, G. Cerullo, and G. Lanzani (CRC Press, Boca Raton, 2007) pp. 130 – 172.
[42] G. C. Cho, T. Dekorsy, H. J. Bakker, R. Hövel, and H. Kurz, Phys. Rev. Lett. **77**, 4062 (1996).
[43] M. Hase, S. Nakashima, K. Mizoguchi, H. Harima, and K. Sakai, Phys. Rev. B **60**, 16526 (1999).
[44] Y.-M. Chang, Appl. Phys. Lett. **80**, 2487 (2002).
[45] Y.-M. Chang, Appl. Phys. Lett. **82**, 1781 (2003).
[46] K. Ishioka, A. Basak, and H. Petek, Phys. Rev. B **84**, 235202 (2011).
[47] L. Dhar, J. Rogers, and K. A. Nelson, Chem. Rev. **94**, 157 (1994).
[48] K. Ishioka, M. Hase, M. Kitajima, and H. Petek, Appl. Phys. Lett. **89**, 231916 (2006).
[49] A. V. Kuznetsov and C. J. Stanton, Phys. Rev. B **51**, 7555 (1995).
[50] A. Basak, H. Petek, K. Ishioka, E. Thatcher, and C. Stanton, Phys. Rev. B **91**, 125201 (2015).
[51] J. Sjakste, N. Vast, and V. Tyuterev, Phys. Rev. Lett. **99**, 236405 (2007).
[52] C. M. Collier, B. Born, X. Jin, and J. F. Holzman, Appl. Phy. Lett. **103**, 072106 (2013).
[53] D. Aspnes and A. Studna, Phys. Rev. B **27**, 985 (1983).
[54] S. M. Sze, *Semiconductor Devices, Physics and Technology, 2nd Edition* (Wiley, New York, 2002) p. 176.
[55] M. Hase, M. Katsuragawa, A. M. Constantinescu, and H. Petek, Nat. Photon. **6**, 243 (2012).
[56] M. Hobden and J. Russell, Phys. Lett. **13**, 39 (1964).
[57] W. Kauschke, V. Vorlicek, and M. Cardona, Phys. Rev. B **36**, 9129 (1987).
[58] M. Hase, M. Kitajima, A. Constantinescu, and H. Petek, Nature **426**, 51 (2003).
[59] C. Shih and A. Yariv, J. Phys. C **15**, 825 (1982).
[60] We neglect the time convolution of the probe pulse with $\Delta R[t, N(r)]$ since the 10 fs temporal width of the laser pulse is small compared to the typical ps dynamic time scale.

FIGURES

FIG. 1. (Color Online.) (a) The band structure of GaP near the fundamental band gap, based on a 30 band $\vec{k}\cdot\vec{P}$ calculation[27,28]. The parameters are optimized to fit the band structure calculation of Chelikowsky and Cohen[29]. The solid and broken arrows indicate the major transitions with 3.1-eV photons and intervalley scatterings. Direct excitation occurs only into the Γ valley, where the carriers scatter into the satellite X and L valleys. (b) Plasma frequency ν_p for the electrons in Γ, X, L valleys, the light and heavy holes, and the mixed plasma, of GaP as a function of carrier density. The masses used to determine ν_p are given in Table I. The mixed plasma mass $m_{\rm eh}$ stands for the combined heavy hole and X valley electron mass, *i.e.*, $m_{\rm eh}^{-1} = m_{\rm HH}^{-1} + m_{\rm X}^{-1}$. LO and TO phonon frequencies are indicated by the broken lines in (b).

FIG. 2. (Color Online.) Schematic energy diagram of an n-doped polar semiconductor surface. (a) Fermi level ($E_{\rm Fermi}$) is pinned near the mid-gap at the surface, leading to the upward bending of the conduction band minimum (CBM) and the valence band maximum (VBM) toward the surface in the surface depletion layer. (b) Upon illumination with a femtosecond optical pulse, photoexcited electrons and holes drift to opposite directions and screen the surface field. This suddenly shifts the nuclear equilibrium positions and thereby launches coherent LO phonons and LOPC modes via the TDFS mechanism. (c) After screening is completed, both electrons and holes diffuse away from the surface (ambipolar diffusion) on sub-picosecond time scale.

FIG. 3. (Color Online.) Pump polarization-dependence of the amplitudes $\Delta R_{\rm LO}/R$ and $\Delta R_{\rm LOPC}/R$ for n-doped GaP pumped and probed at 800 nm (a) and 400 nm (b). The probe polarization is fixed to be parallel to the [100] axis (45° from vertical) for the EO detection. Solid curves show the fitting of the amplitudes to $A + B\cos 2\theta$.

FIG. 4. (Color Online.) Oscillatory parts of anisotropic reflectivity changes $\Delta R_{eo}/R$ (a-c) and their FT spectra (d-e) pumped and probed with 400-nm light at different pump energy densities F: for n-doped (a,d), undoped (b,e) and p-doped (c,f) GaP. Traces in (a-c) are offset for clarity. The LO and TO phonon frequencies are indicated by broken lines in (d-f).

FIG. 5. (Color Online.) Carrier density-dependence of the frequencies (a) and the dephasing rates (b) of the LOPC and LO modes of differently doped GaP pumped and probed with 400-nm light. Solid curve represent the calculated LOPC frequency and dephasing rate in Fig. 8 in the case of $\gamma_p/2\pi$=25 THz. The LO and TO phonon frequencies are indicated by broken lines in (a).

FIG. 6. (Color Online.) Carrier density-dependence of amplitudes $\Delta R_{\rm LOPC}/R$ (a) and $\Delta R_{\rm LO}/R$ (b) for differently doped GaP pumped and probed with 400-nm light. Broken curves are to guide the eye.

FIG. 7. (Color Online.) Time-windowed FT amplitudes of the reflectivity oscillations as functions of time window position and frequency: for n-doped (a), undoped (b) and p-doped (c) GaP. A Gaussian time window with 200 fs half width is used. Dots represent the spectral peak position at each time window. Carrier density is $1.7 \pm 0.2 \times 10^{19}$ cm^{-3}. The LO and TO phonon frequencies are indicated by broken lines.

FIG. 8. (Color Online.) Calculated coupled mode frequency $\mathrm{Re}(\omega)/2\pi$ (a) and dephasing rate $\mathrm{Im}(\omega)/2\pi$ (b) as a function of carrier density for different plasma damping rate ranging from $\gamma_p/2\pi$=5 to 40 THz. Equation (5) is numerically solved using the mixed plasma effective mass $m_{\rm eh} = 0.22m_0$ and the phonon damping $\Gamma/2\pi$=0.04 THz. The LO and TO phonon frequencies are indicated by broken lines in (a).

FIG. 9. (Color Online.) Normalized carrier density $N(t, z = 0)/N_0$ (a) and LOPC frequency $\mathrm{Re}(\omega)/2\pi$ at surface calculated as a function of time in the case of the diffusion coefficients of $D_{\rm am}$=5 and 10 cm^2 s^{-1}. The effective mass of $m_{\rm eh} = 0.22m_0$, plasma damping of $\gamma_p/2\pi$ =24 THz, and carrier density of $N_0 = 2 \times 10^{19}$ cm^{-3} are used. The LO and TO phonon frequencies are indicated by broken lines in (b).

FIG. 10. (Color Online.) Reflectivity changes ΔR calculated for different carrier densities N_{max} with lateral density inhomogeneity taken into account. Plasma and phonon damping rates of $\gamma_p/2\pi$=24 THz and $\Gamma/2\pi$= 0.04 THz are used. Carrier diffusion is not included in the calculations. Traces in (a) are offset for clarity. The LO and TO phonon frequencies are indicated by broken lines in (b).

FIG. 11. (Color Online.) Time-windowed FT spectra of the calculated reflectivity changes for the carrier density of 2×10^{19} cm^{-3}. Carrier density inhomogeneity arising from the laser spot profile is neglected in (a) but taken into account in (b). Diffusion is neglected in both (a) and (b). Gaussian time window of 200 fs half width is used. Dots represent the spectral peak position at each time window. The LO and TO phonon frequencies are indicated by broken lines.

TABLES

TABLE I. Effective masses of the electrons and holes of GaP in units of m_0. m_l and m_t are the longitudinal and transverse masses for the conduction electrons in the ellipsoidal L and X valleys, and m^* is the optical effective mass defined by $m^{*-1} = (2/3)m_t^{-1} + (1/3)m_l^{-1}$. $m_{\rm HH}$ and m_X denote the effective masses for the heavy holes and the electrons in the X valley.

Valley	m_l	m_t	m^*
Γ electron			0.09
L electron	1.2	0.15	0.21
X electron	1.12	0.22	0.30
Light hole			0.14
Heavy hole			0.79
mixed plasma ($m_{\rm eh}^{-1} = m_{\rm X}^{-1} + m_{HH}^{-1}$)			0.22

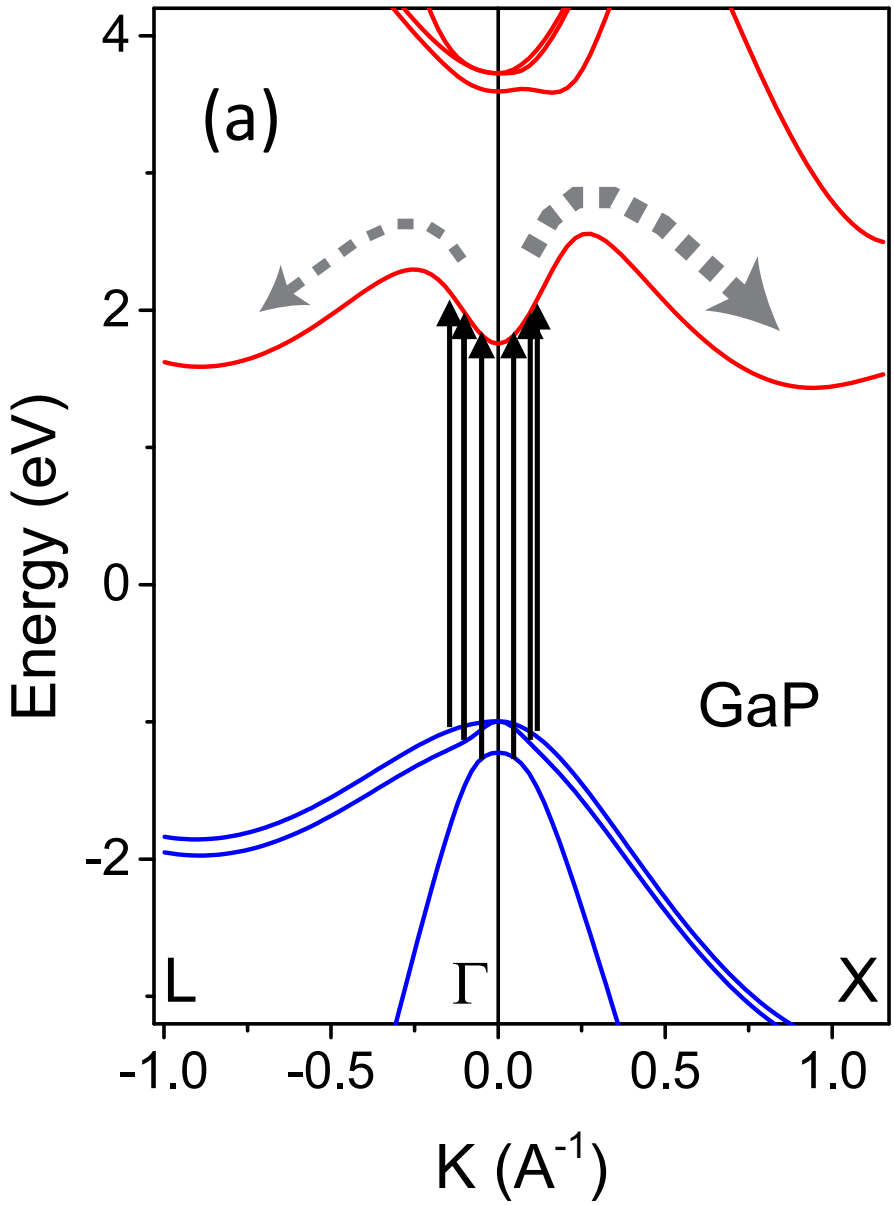

Figure 1a 14Oct2015

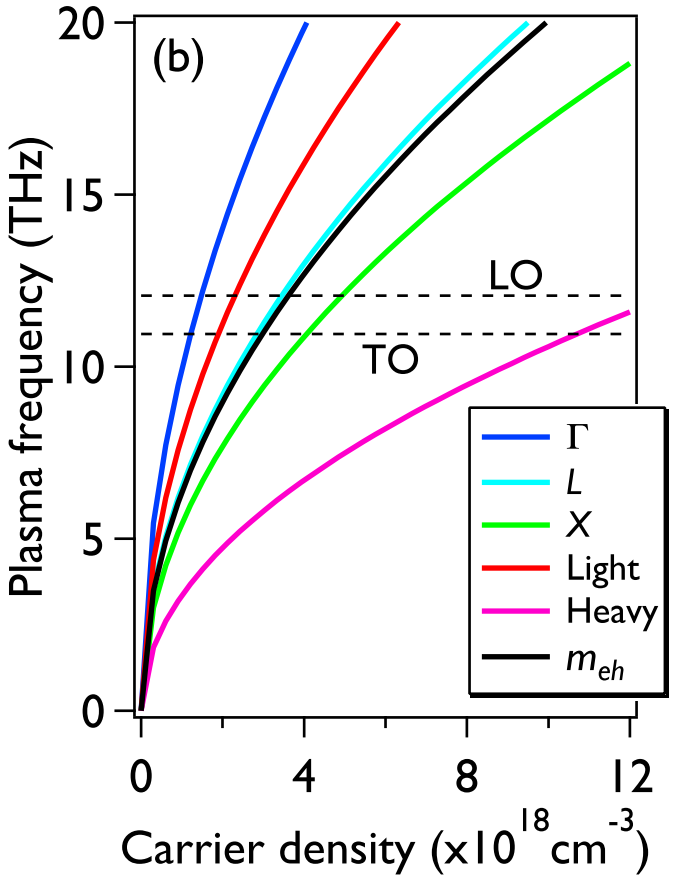

Figure 1b 14Oct2015

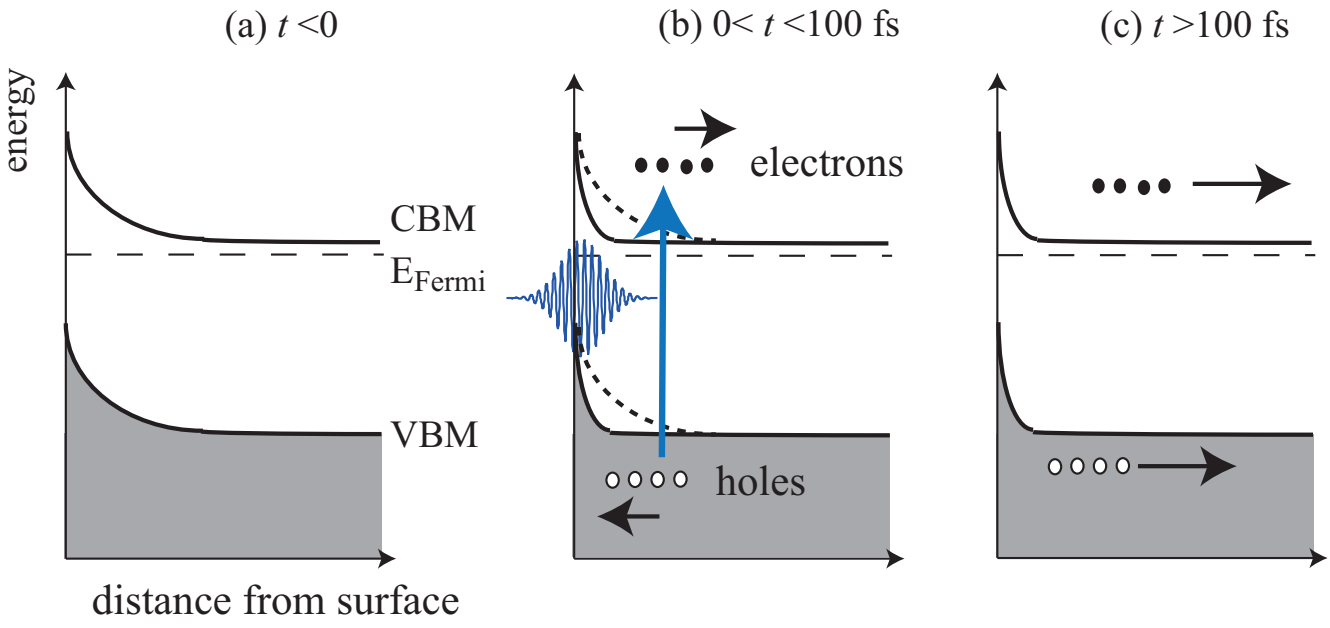

Figure 2 14Oct2015

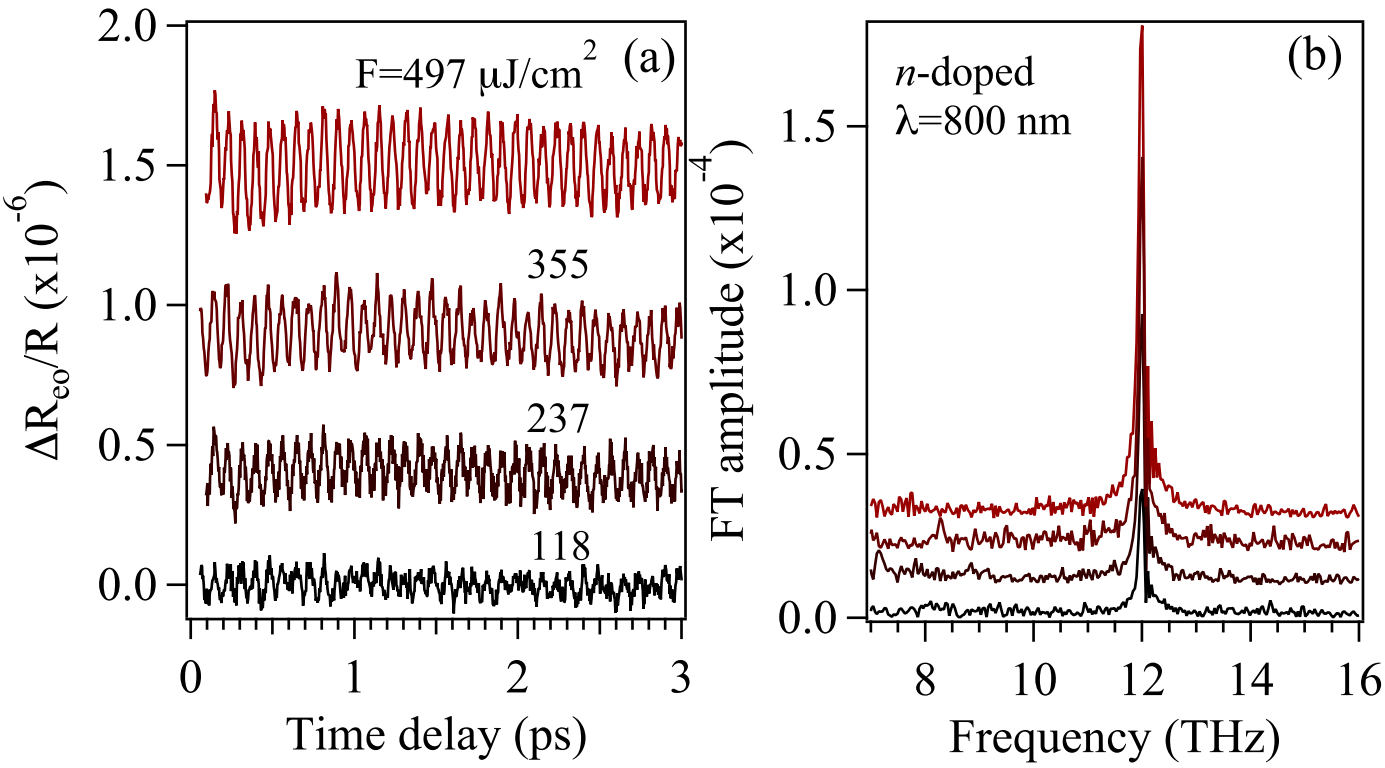

Figure 3 14Oct2015

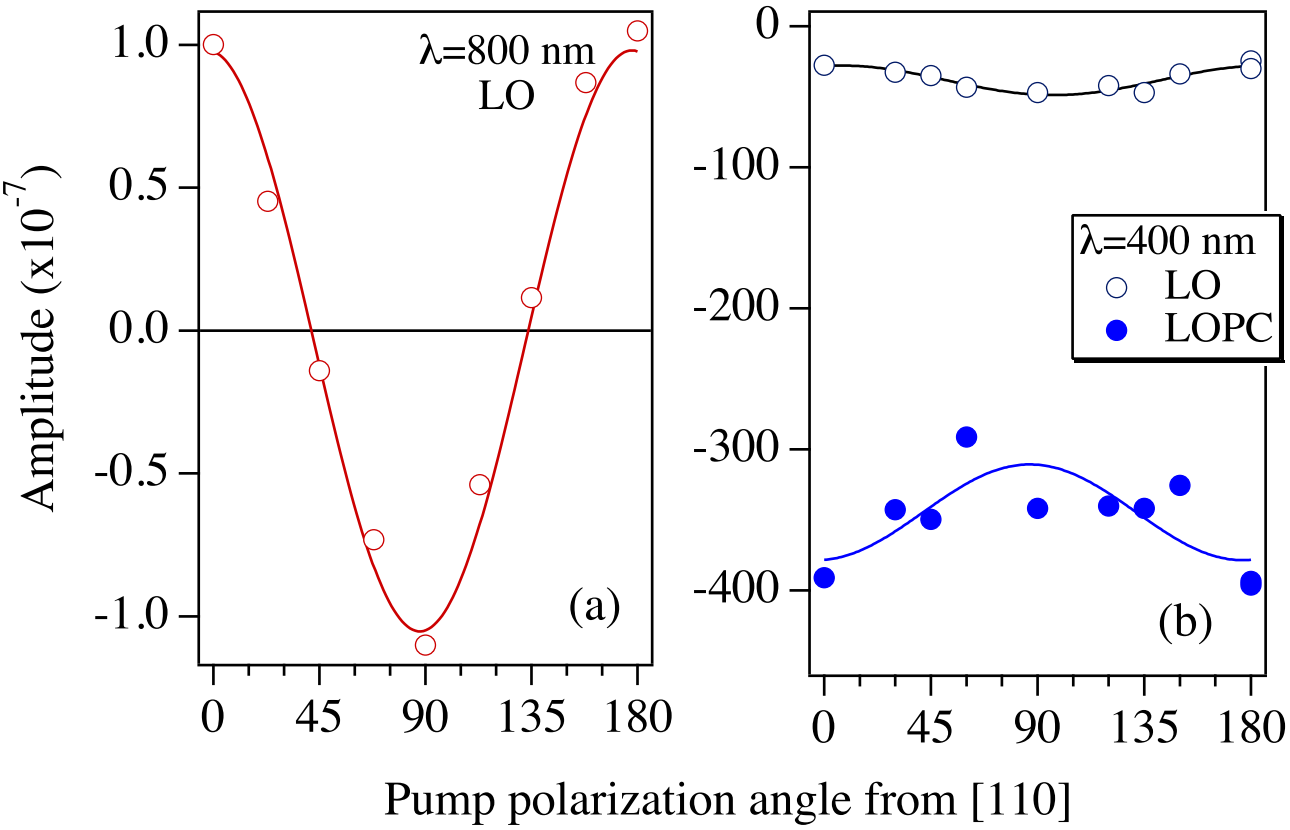

Figure 4 14Oct2015

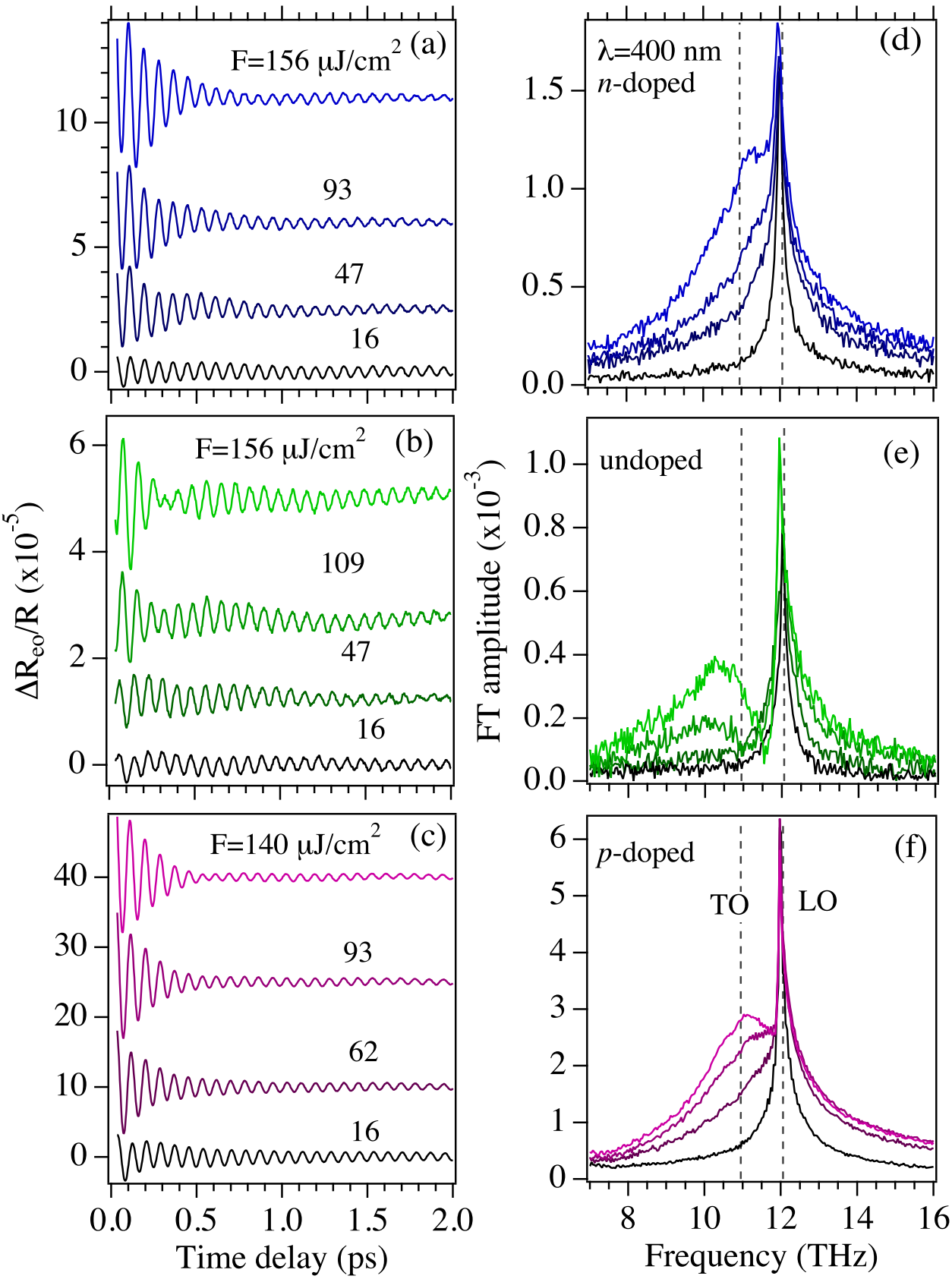

Figure 5 14Oct2015

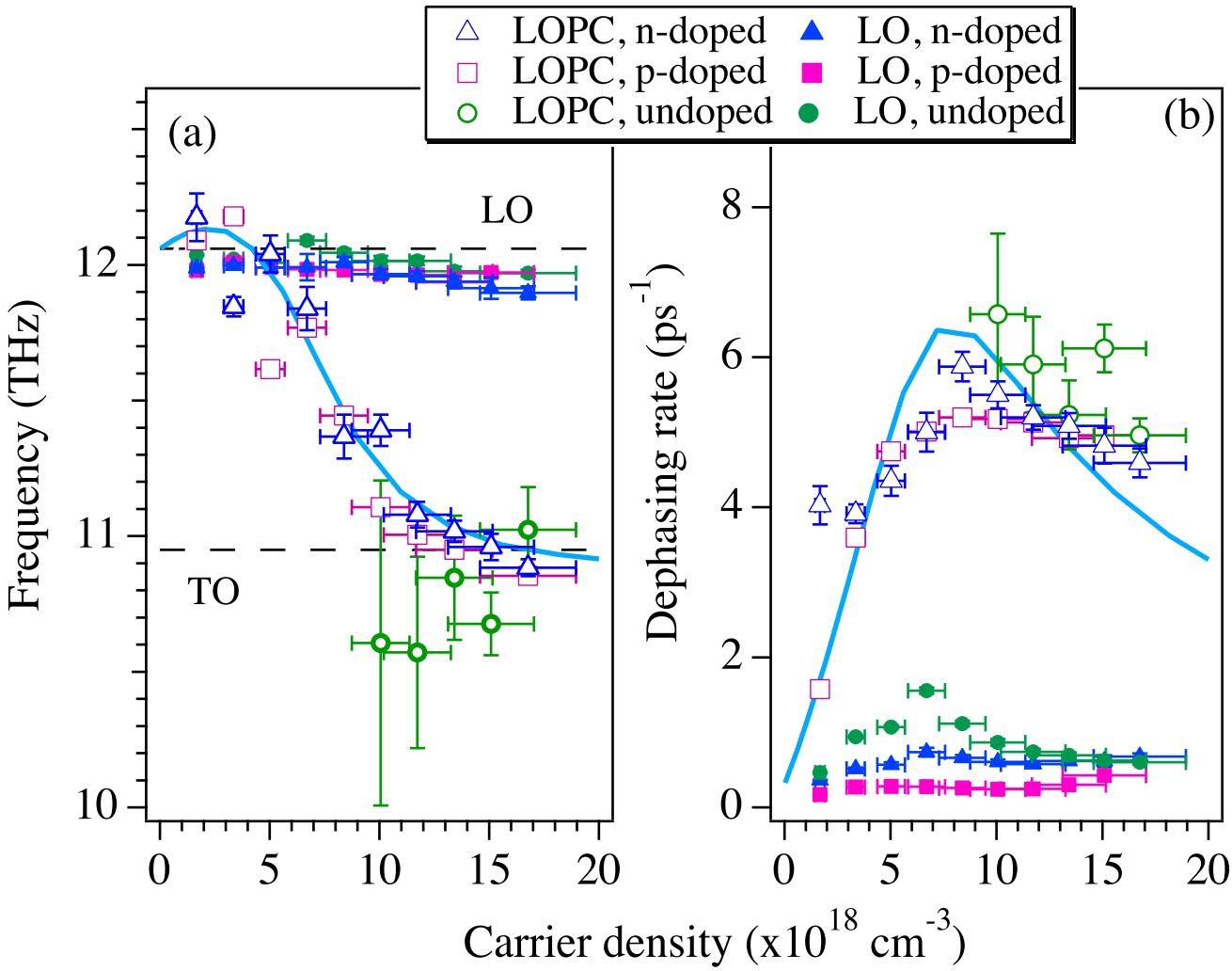

Figure 6 14Oct2015

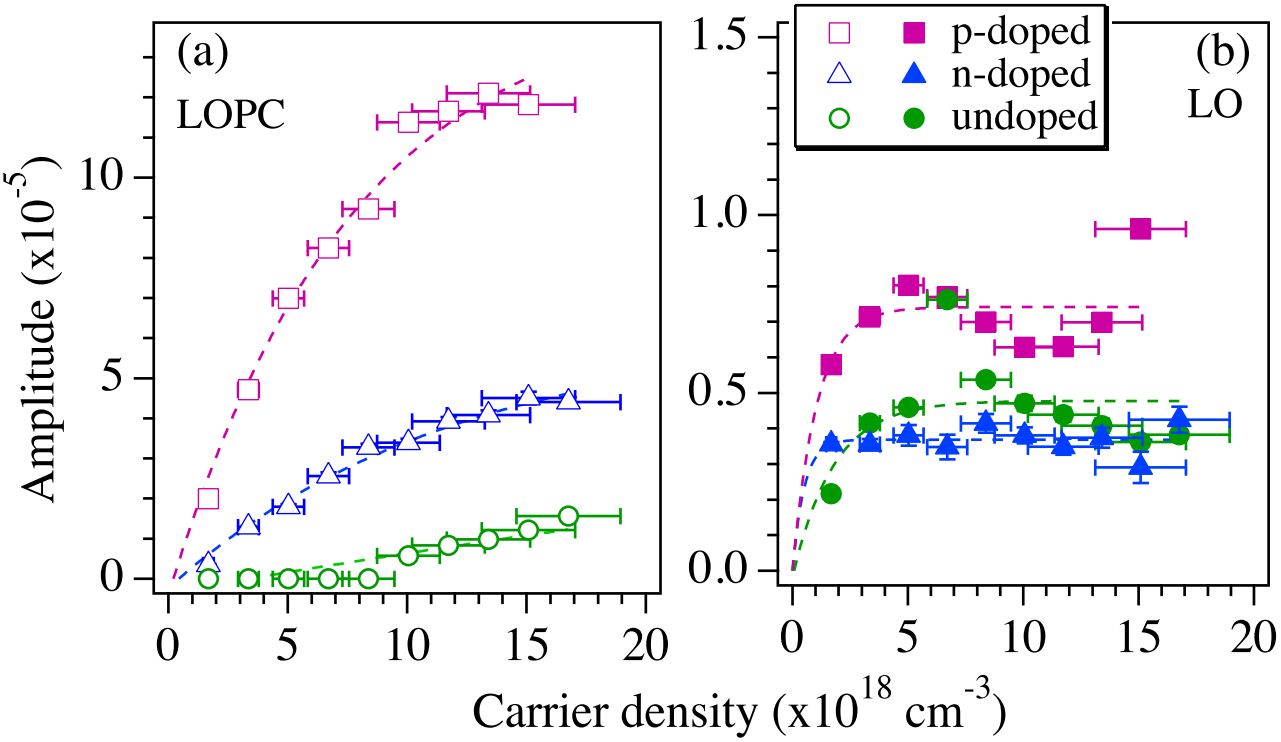

Figure 7 14Oct2015

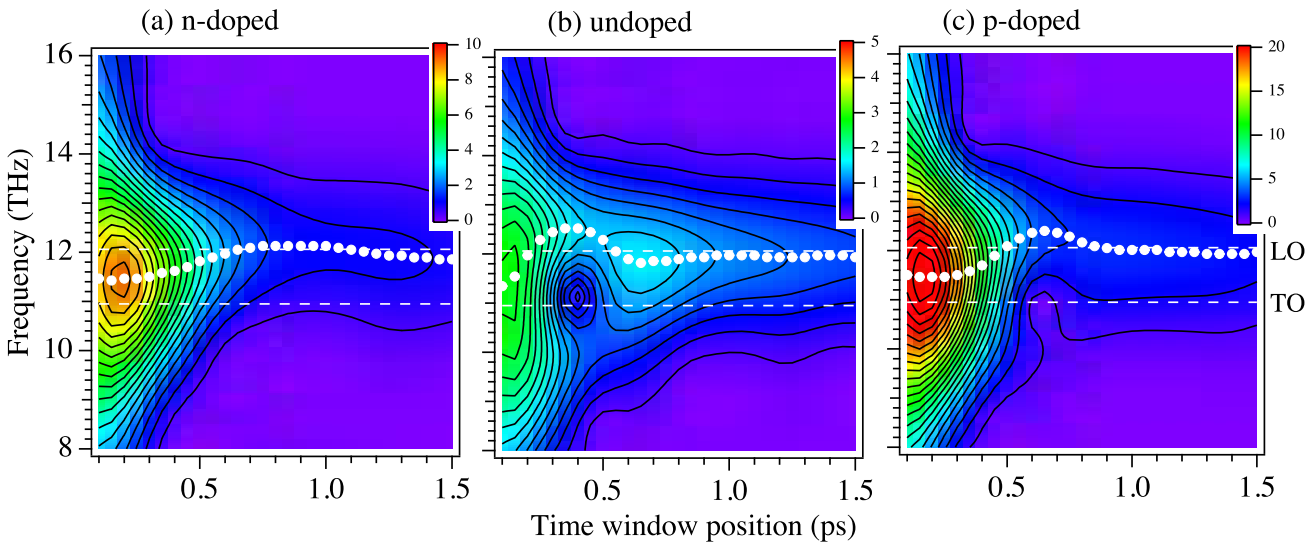

Figure 8 14Oct2015

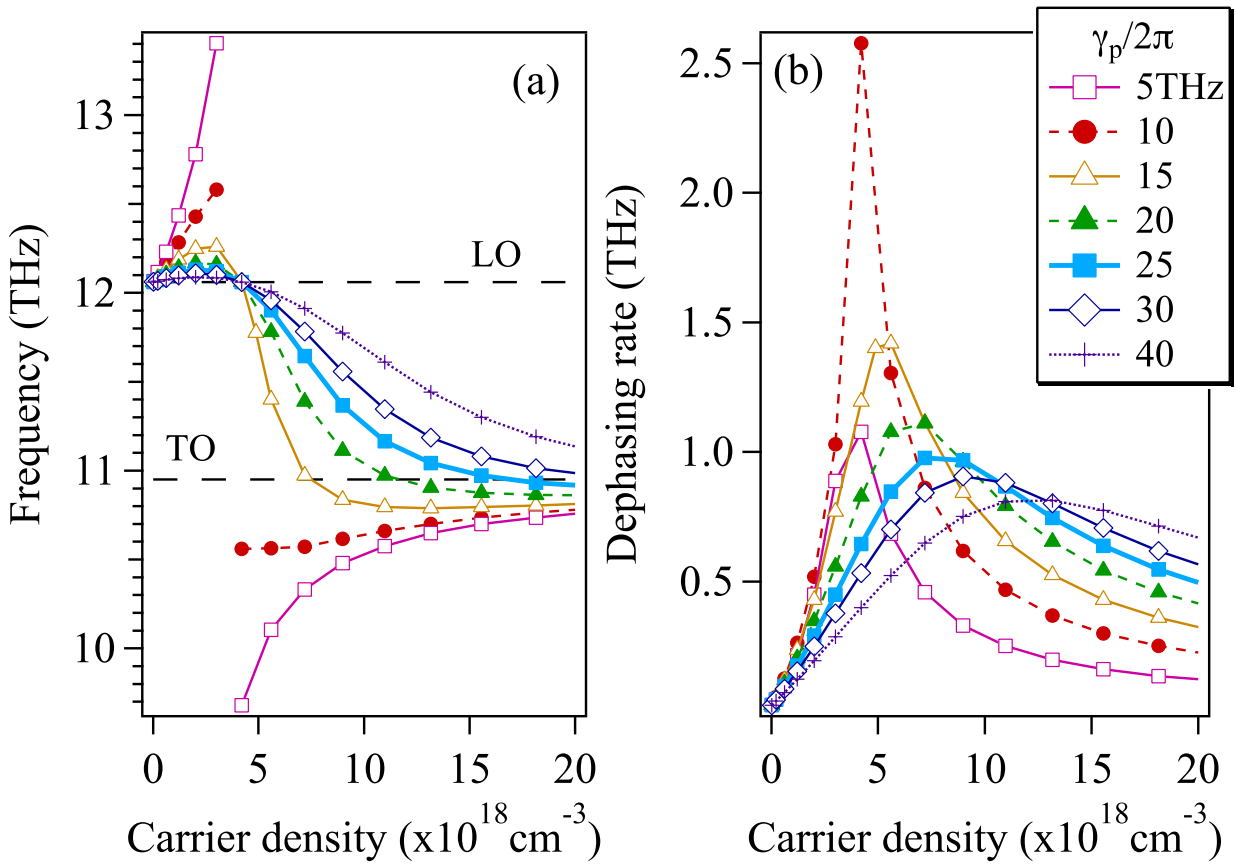

Figure 9 14Oct2015

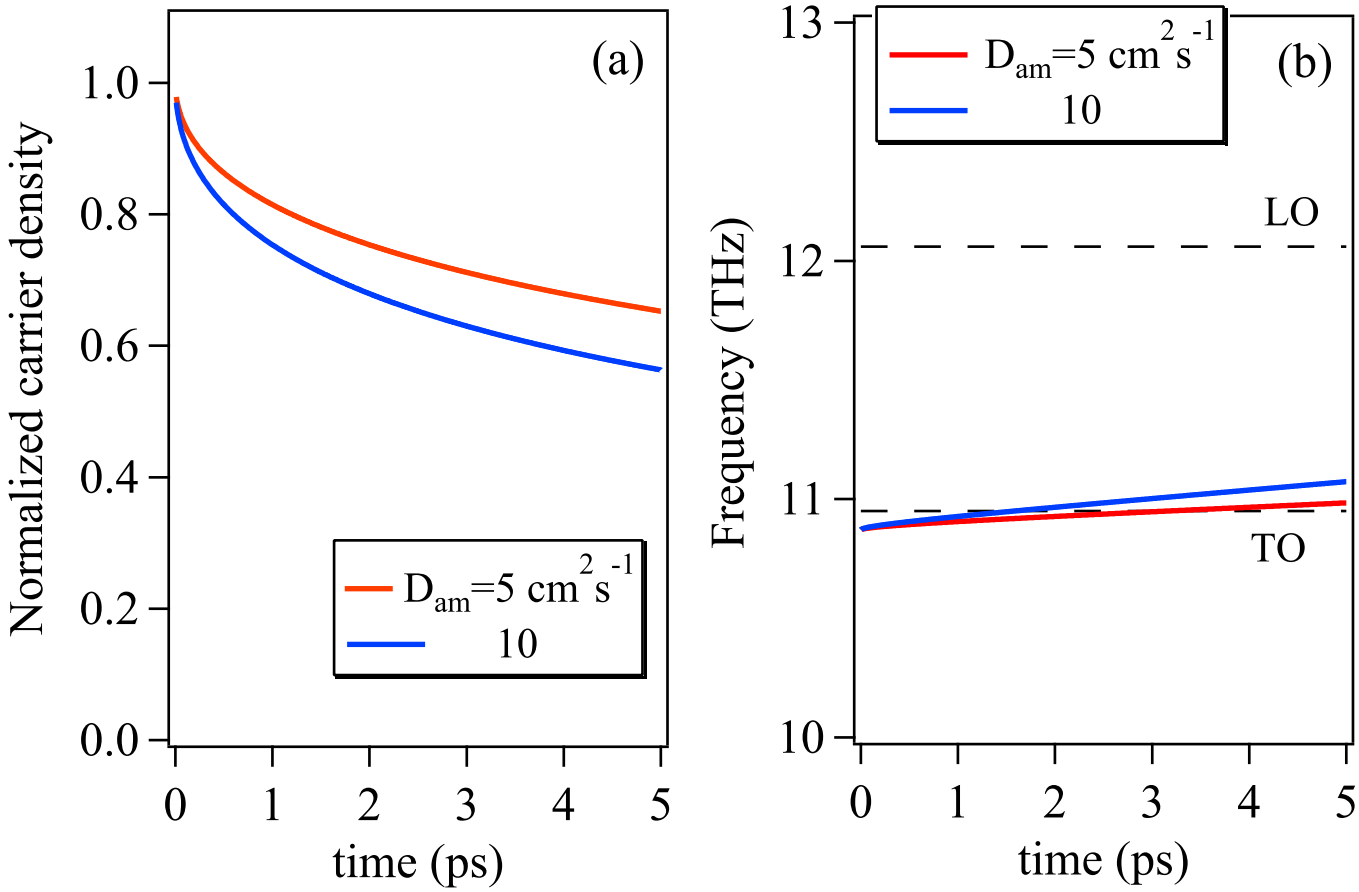

Figure 10 14Oct2015

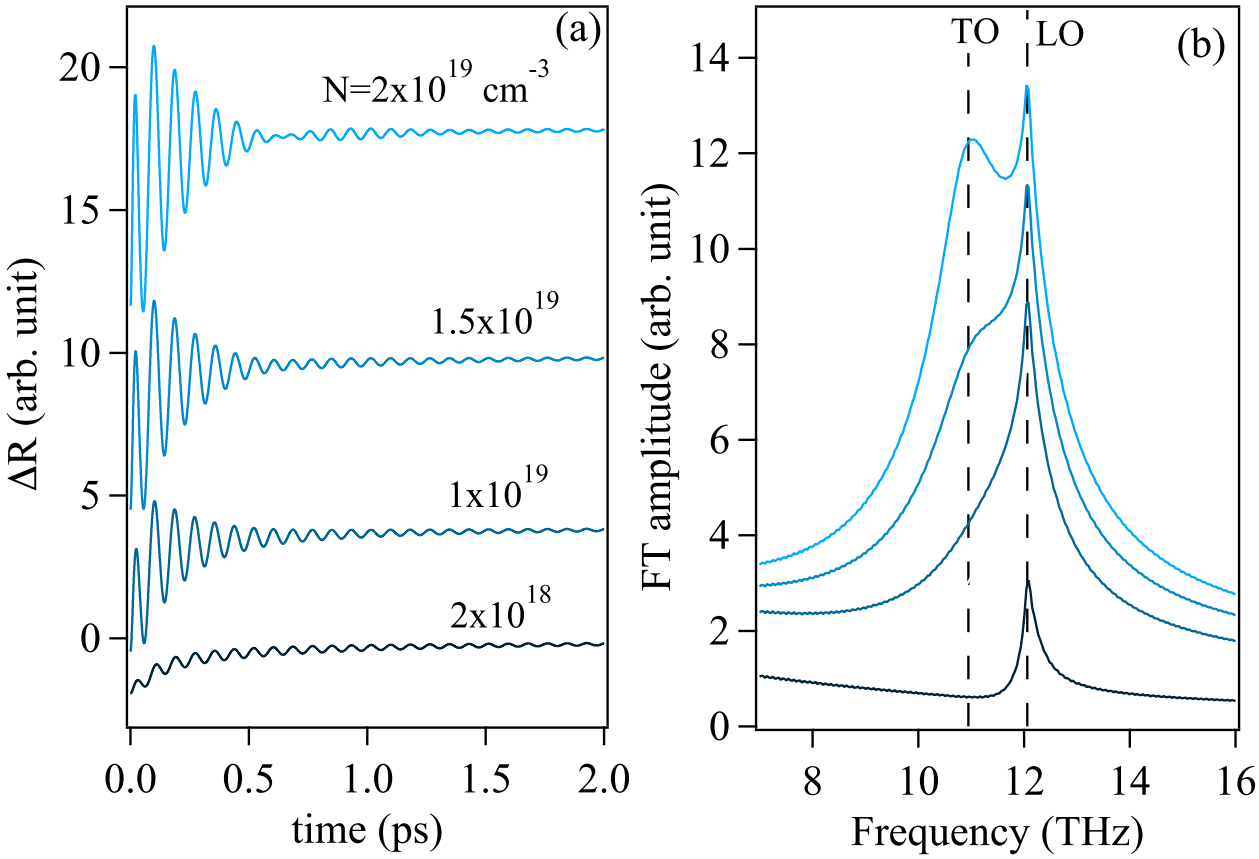

Figure 11 14Oct2015

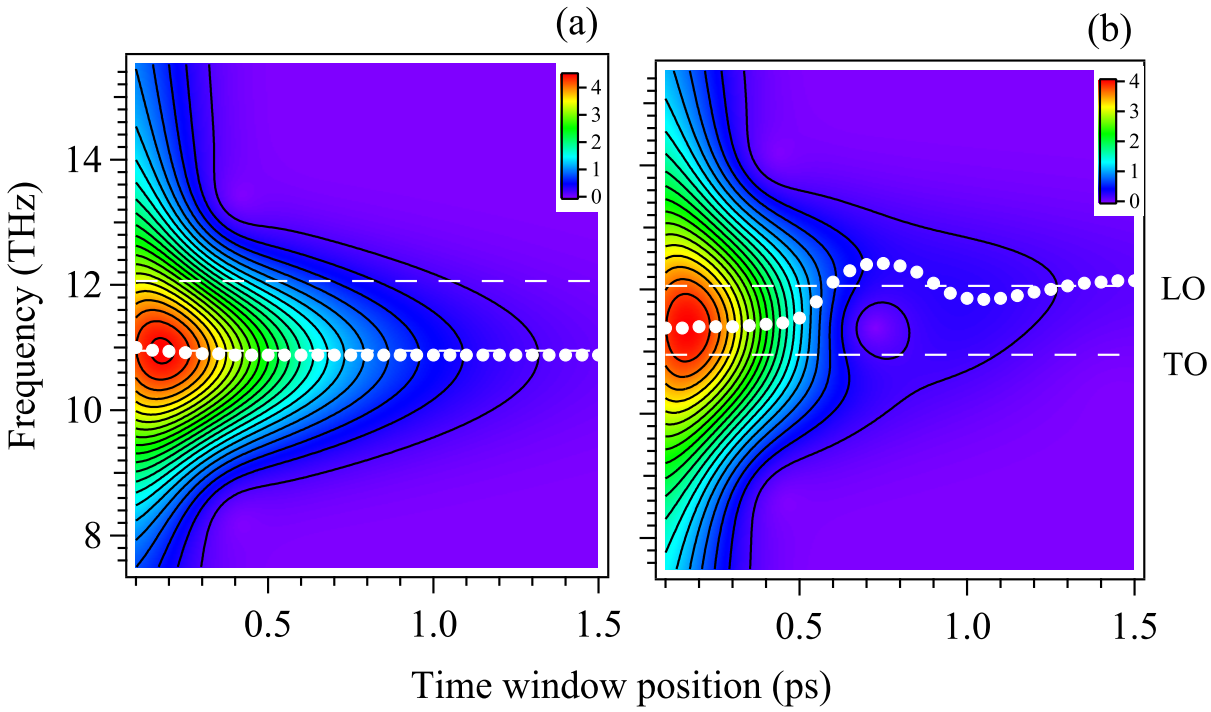

Figure 12 14Oct2015